Preliminary Design and Performance Assessment of a Solar Electric Catamaran for Okrika Inland Waterway

Christian Jumbo, Samson Nitonye, Morrison Inegiyemiema
Department of Marine and Offshore Engineering,
Rivers State University,
Port Harcourt, Rivers State, Nigeria

https://doi.org/10.56201/ijemt.vol.12.no11.2026.pg10.23

Abstract
Solar electric propulsion offers a means of reducing dependence on onboard combustion engines for inland passenger and crew transport, but its feasibility depends on the relationship between hull resistance, available photovoltaic area, seasonal solar energy and energy storage. This study develops a preliminary numerical assessment of a 24 m long, 8.5 m wide catamaran proposed for Okrika inland waterway, Nigeria. The analysis combines a six-series monthly solar input matrix, reported ANSYS AQWA hydrostatic and hydrodynamic results, a reproducible calm-water resistance model and an illustrative twin-propeller matching calculation. The assumed full-area photovoltaic installation has a theoretical peak capacity of 61.2 kW at 30% conversion efficiency. Recalculation of the solar matrix gives an unweighted mean of 4.22 peak sun hours per day and approximately 258.29 kWh/day before losses. At the selected speed of 5.4 knots, the resistance model predicts approximately 1.95 kN resistance and 11.17 kW electrical propulsion demand. Two nominal 1.0 m propellers at 189 rpm give a predicted matching speed of approximately 5.44 knots. The reported hydrostatic solution gives 56.54 m³ displacement volume and 19.10 m transverse metacentric height, while the principal natural modes lie between 0.372 and 0.495 Hz. A sensitivity calculation shows that a 22% module-efficiency assumption with 80% usable area reduces theoretical photovoltaic capacity to 35.90 kW. The results support further development of a moderate-speed solar-assisted vessel concept.

Keywords: *solar electric propulsion; catamaran; photovoltaic energy; vessel resistance; propeller matching; marine energy storage.*

1 Introduction

Passenger and crew transport on inland waterways require a propulsion system that can meet scheduled demand while limiting operating costs and local exhaust emissions. Photovoltaic generation and battery storage provide an alternative energy pathway: sunlight is converted into electricity, stored when generation exceeds demand and delivered to electric motors when propulsion is required. The engineering question is whether sufficient usable energy can be carried and replenished within the vessel's available area, displacement and operating schedule. A peak photovoltaic rating alone cannot answer this question. Catamarans provide a useful configuration for examining this problem because the connecting deck can support a relatively broad solar canopy and the separated hulls permit distributed machinery and storage (Nitonye et al., 2020).

The same arrangement introduces design interactions. A wider canopy increases wind loading; batteries alter displacement and centre of gravity; and hull spacing influences wave interference, structural loading and transverse stability. Consequently, electrical sizing should develop alongside the hull and propulsion design rather than after the vessel geometry has been fixed. Schirripa Spagnolo et al. (2012) similarly linked solar-canopy layout, battery storage and electric propulsion in a tourist-boat concept, illustrating the importance of treating these elements as one design problem. Nasirudin, Chao and Utama (2017) presented a solar-boat design methodology that links ship dimensions, propulsion requirements and photovoltaic sizing. Their work supports the use of an integrated design process in which reductions in resistance can be as valuable as increases in generation capacity. Han, Charpentier and Tang (2014) examined energy management in a fuel-cell/battery hybrid boat, demonstrating the relevance of coordinated source and storage control to marine propulsion. Although their energy source differs from photovoltaics, the need to balance variable supply, storage state and motor demand remains pertinent.

Geertsma et al. (2017) reviewed hybrid ship power and propulsion arrangements and emphasised the interaction between system architecture and control. For the present application, this means that motor capacity, battery capacity and solar capacity cannot be selected independently. A motor must satisfy the demanded torque and speed, while the storage system must accommodate both energy deficits and short-duration power requirements. The photovoltaic array determines the rate at which renewable energy can replenish that storage. Moya et al. (2022) analysed the INER 1 solar catamaran using environmental, passenger and energy variables; this supports recording the operating conditions alongside energy consumption in future trials.

The present work addresses four connected questions. First, what daily energy follows from the proposed photovoltaic area and supplied solar inputs? Second, what hydrostatic and first-order motion characteristics are reported for the catamaran? Third, what propulsion demand is predicted across the operating-speed range? Fourth, does the proposed twin-propeller arrangement match the hull near the selected cruise speed? These questions establish a preliminary operating envelope and expose the principal uncertainties affecting the design.

The central contribution is an integrated assessment of generation, propulsion and vessel response at a consistent operating point. The analysis distinguishes installed peak power from daily energy, reconciles two different propulsion-efficiency formulations and identifies the evidence needed to progress from a numerical concept to an operational craft. All calculated performance values are predictions; no prototype trial or measured fuel-saving result is claimed.

2.0 Materials and methods

The vessel is represented as a fibreglass-polyester catamaran with a nominal overall length of 24 m, beam of 8.5 m and modelled displacement mass of 57,955.23 kg. The resistance calculation adopts 24 m as the waterline length. This is a modelling assumption requiring confirmation from the final lines plan. A 5.4-knot cruise speed is used consistently for the principal comparison.

Table 1. Principal numerical inputs and their status.

Parameter	Value
Length used in resistance model	24.0 m
Overall beam	8.5 m
Displacement mass	57,955.23 kg
Wetted surface area	135 m²
Gross horizontal area	204 m²
Selected cruise speed	5.4 knots
Seawater density	1,025 kg/m³
Kinematic viscosity	1.19×10^{-6} m²/s
Propeller arrangement	Twin 1.0 m diameter
Motor reference speed	1,000 rpm

Solar input treatment

The solar matrix contains 12 monthly entries for each of six series. Its code labels the series 2015–2020, whereas the results narrative uses 2020–2025 and contains mixed year references. Because the underlying measurement source and calendar labels cannot be established, the series are analysed without definitive year attribution. Monthly means and the unweighted mean of all 72 entries are used as design inputs. They should not be interpreted as a verified climatological record for Okrika. The workflow first calculates photovoltaic peak capacity and monthly energy, then evaluates resistance and electric power against speed. Reported hydrostatic and seakeeping quantities are assessed for consistency with the intended service. Finally, propeller thrust is compared with the hull requirement at a fixed shaft speed. No statistical confidence interval is assigned because the input uncertainties and measurement errors have not been characterised.

Resistance and propulsion model

The calculation separates viscous resistance with a form correction, an assumed residual-resistance contribution and a correlation allowance. Water speed V is expressed in m/s, using 0.514444 m/s per knot. Reynolds and Froude numbers are obtained from the adopted waterline length L, kinematic viscosity ν and gravitational acceleration g. The ITTC-1957 friction line is used in the form documented in standard ship-hydrodynamics practice (Bertram, 2012; Nitonye and Adumene, 2015). The International Towing Tank Conference (ITTC, 2021a) provides the broader framework for extrapolating resistance and propulsion test results to full-scale performance; applying the friction line alone does not constitute completion of that procedure.

$$R_n = VL/\nu\,;\; F_n = V/\sqrt{gL}\,;\; C_F = 0.075/[\log_{10}(R_n) - 2]^2 \quad (1)$$

The residual coefficient is an illustrative expression supplied with the numerical model. It introduces a gradual speed-dependent term and a sharper rise around a Froude number of 0.30. It has not been calibrated against towing-tank or computational-fluid-dynamics results for this hull.

The coefficient 1.08 provisionally represents interaction between the two hulls, rather than a validated catamaran interference law.

$$C_r = 1.08\{0.00025 + 0.0008(F_n/0.25)^3 + 0.005/[1 + e^{-u}]\} \quad (2)$$
$$u = (F_n - 0.30)/0.025$$

Using wetted area S = 135 m², form factor k = 0.15 and allowance CA = 0.0004, total resistance is calculated from Equation (3). These assumptions are retained to reproduce the design calculations; the resulting curve is suitable for screening and sensitivity assessment, not final motor procurement.

$$R_T = \tfrac{1}{2}\rho V^2 S[(1 + k)C_F + C_r + C_A] \quad (3)$$

Effective power is the rate of work required to overcome total resistance. Delivered power and electrical input are obtained using the assumed propulsive coefficient of 0.55, shaft efficiency of 0.97 and motor/controller efficiency of 0.91. The same convention is retained at every speed to permit consistent comparison.

$$P_E = R_T V/1000\,;\ P_D = P_E/0.55\,;\ P_{el} = P_D/(0.97 \times 0.91) \quad (4)$$

All powers in Equation (4) are in kilowatts when resistance is in newtons. The aggregate coefficient from electrical input to effective power is 0.4855. Auxiliary loads are excluded from Pel and must be added separately (Nwaorgu and Ogbonnaya, 2023). Wind resistance, shallow-water effects, current-related changes in required water speed and added resistance in waves are not included. The calculation therefore represents idealised calm-water operation.

Propeller matching formulation

For twin identical propellers, the total thrust requirement is RT/(1 − t), where thrust deduction t = 0.10. Wake fraction w = 0.15 gives advance velocity VA = V(1 − w). With diameter D = 1.0 m and shaft speed n in revolutions per second, the advance coefficient is J = VA/(nD). The preliminary open-water polynomials are KT = 0.28 − 0.19J − 0.05J² and KQ = 0.042 − 0.026J − 0.007J². These are illustrative curves, not verified manufacturer or Wageningen-series data. ITTC (2021b) describes open-water tests for determining propeller thrust and torque characteristics. Such measurements are required to replace the assumed polynomials.

$$T = 2\rho n^2 D^4 K_T\,;\ Q_{each} = \rho n^2 D^5 K_Q\,;\ \eta_0 = JK_T/(2\pi K_Q) \quad (5)$$

Photovoltaic energy and storage formulation

The baseline assumes that the full 24 m × 8.5 m horizontal envelope is available for photovoltaic conversion. At irradiance G = 1 kW/m² and efficiency ηPV = 0.30, theoretical peak output is 61.2 kW. This is an area-based upper estimate rather than a confirmed installed rating: access routes, module spacing, equipment shading, mounting geometry and the difference between cell and complete-module efficiency have not been resolved. King, Boyson and Kratochvil (2004) include irradiance, temperature and optical effects in photovoltaic performance modelling. These effects should be represented when converting the theoretical area-based estimate into a realistic generation model.

$$P_{PV} = A\eta_{PV}G\,;\ E_{day} = P_{PV}H\,;\ E_{usable} = PR \times E_{day} \quad (6)$$

H denotes peak sun hours per day and PR denotes an assumed aggregate photovoltaic yield factor. A value of 0.80 is used only as a sensitivity scenario for generation-side losses. It is not a measured performance ratio. Motor and shaft losses remain within Equation (4); storage losses are considered separately when energy passes through the battery. This boundary prevents counting the same loss twice. Dobos (2014) distinguishes rated capacity from simulated energy yield and explicitly models photovoltaic system losses. The present 0.80 factor is a simplified scenario, not a PVWatts simulation.

Battery capacity must be selected from the voyage energy deficit, reserve requirement, usable depth of discharge and discharge-path efficiency. For a no-solar interval of duration τ, a preliminary nominal-energy requirement is expressed by Equation (7). Paux is the auxiliary load and r is an energy reserve fraction. Charge-rate, thermal and power limits require separate checks. Schirripa Spagnolo et al. (2012) also emphasise battery charge management and operating autonomy in solar-electric boat design.

$$E_{nom} \geq (P_{el} + P_{aux})\tau(1 + r)/(DoD \times \eta_{dis}) \quad (7)$$

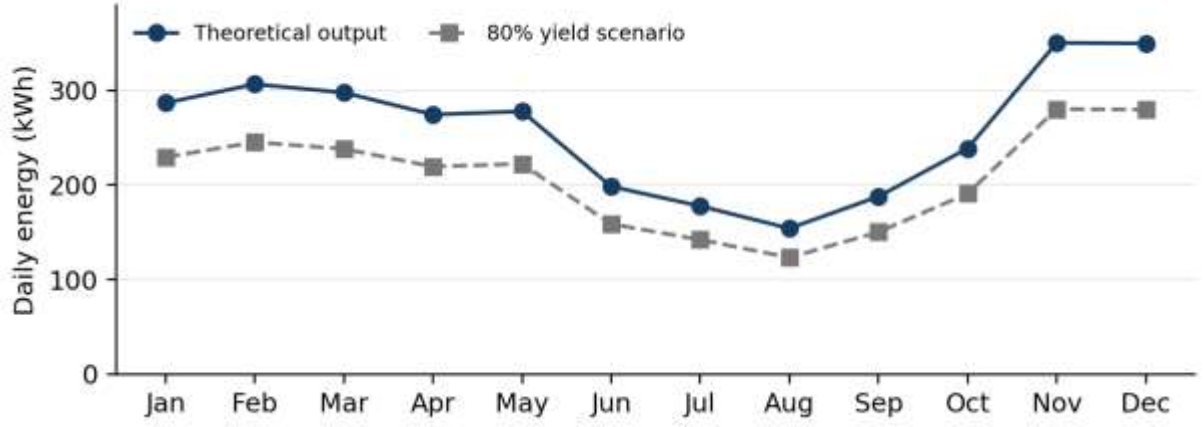


Figure 1. Recalculated monthly energy from the supplied solar matrix at 61.2 kW theoretical peak capacity. The 80% curve is an assumed yield scenario.

For illustration only, using 11.17 kW propulsion, 2.0 kW auxiliaries, two hours without solar input, 20% reserve, 80% allowable discharge and 90% discharge-path efficiency gives approximately 43.9 kWh nominal storage.

3.0 Results and Discussion

Recalculation gives an unweighted average of 4.2204 peak sun hours per day. The corresponding theoretical energy is 258.29 kWh/day, compared with approximately 258.26 kWh/day reported using rounded intermediate values. Multiplication by the illustrative 0.80 yield factor gives 206.63 kWh/day before any additional battery-path losses. The average is not weighted by the different numbers of days in each month.

Table 2. Monthly mean solar inputs and calculated energy availability.

Month	Peak sun hours	Theoretical kWh/day	80% scenario kWh/day
Jan	4.685	286.72	229.38
Feb	5.008	306.51	245.21
Mar	4.863	297.64	238.11
Apr	4.483	274.38	219.50
May	4.538	277.75	222.20
Jun	3.242	198.39	158.71
Jul	2.903	177.68	142.15
Aug	2.518	154.12	123.30
Sep	3.068	187.78	150.23
Oct	3.900	238.68	190.94
Nov	5.723	350.27	280.21
Dec	5.712	349.55	279.64

November has the highest monthly mean, approximately 5.723 h/day, corresponding to 350.27 kWh/day. August has the lowest mean, approximately 2.518 h/day, giving 154.12 kWh/day. The August mean is about 56% below the November mean. This seasonal contrast is more important for storage and scheduling than the apparent adequacy of annual-average generation.

The smallest individual entry is 1.3 peak sun hours per day. It produces only 79.56 kWh/day theoretically, or 63.65 kWh/day in the 80% yield scenario. Thus, an average daily generation surplus does not guarantee reliable service during a low-resource period. Consecutive cloudy days cannot be evaluated from monthly averages; an hourly or daily time series is required to estimate energy-shortfall probability. Moya et al. (2022) demonstrate the relevance of environmental and operational variability to solar-catamaran energy analysis. The supplied monthly averages cannot resolve the corresponding short-term variations.

At 5.4 knots, eight hours of modelled propulsion requires approximately 89.36 kWh. Adding the illustrative 2 kW auxiliary load raises demand to 105.36 kWh/day. The August-average 80% generation scenario leaves approximately 17.94 kWh before storage losses. Under the minimum-entry scenario, the same schedule produces a deficit of approximately 41.71 kWh. Stored energy, supplementary charging or a reduced schedule would then be necessary.

Hydrostatic equilibrium and initial stability

The reported AQWA model uses a freely floating body of 57,955.2345 kg in water of density 1,025 kg/m³. Its displaced volume is 56.541676 m³. Multiplying volume by density gives approximately 57,955.22 kg, in close agreement with the assigned mass. This confirms numerical buoyancy balance at the modelled condition; it does not establish a complete lightship or operational weight budget.

Table 3. Reported hydrostatic properties and consistency checks.

Quantity	Reported value
Displaced volume	56.541676 m³
Waterplane area	54.748138 m²
Centre of gravity coordinates	(13.4092, 0.03385, 0) m
Centre of buoyancy coordinates	(13.4669, 0.03339, −0.6031) m
Transverse metacentric height	19.102127 m
Longitudinal metacentric height	33.022087 m
Direct heave restoring stiffness	550,318.25 N/m
Roll restoring moment per degree	189,483.91 N·m/degree
Pitch restoring moment per degree	327,563.22 N·m/degree

The longitudinal separation of the reported buoyancy and gravity centres is 0.0577 m. Their transverse separation is 0.00046 m, or 0.46 mm, using the displayed coordinates. This corrects the smaller separation stated in the narrative while preserving the conclusion of near transverse alignment. The vertical coordinates are referenced to the numerical model origin; a centre of gravity at Z = 0 must not be interpreted as a zero height above the keel. The heave stiffness can be checked independently using C33 = ρgAWP. Substitution of the reported waterplane area gives approximately 550.32 kN/m, consistent with the AQWA result. Similarly, the small-angle roll restoring coefficient follows from vessel weight multiplied by transverse metacentric height. These checks support internal consistency of the reported hydrostatic quantities.

A transverse metacentric height of 19.10 m indicates a strong initial restoring tendency under the adopted mass distribution. It does not, by itself, demonstrate adequate stability at large angles. A complete assessment requires a righting-lever curve, downflooding limits, freeboard, loading cases and the effects of passengers, batteries, canopy mass and possible free surfaces. Lewis (1988) distinguishes these broader stability questions from the initial small-angle measure. The high stiffness also has a comfort implication. Restoring rapidly toward upright can produce short natural periods and substantial accelerations. Accordingly, the reported large metacentric height should be considered together with motion response and passenger acceleration rather than used alone as evidence of operational suitability. Faltinsen (2005) discusses the interaction between vessel dynamics, wave excitation and accelerations, supporting a combined assessment of restoring characteristics and seakeeping response.

Hydrodynamic response and model limitations

The reported ANSYS AQWA 2025 R2 analysis uses a nominal 0.45 m element size, 4,036 nodes and 4,051 elements. Frequencies extend from 0.001 to 0.60185 Hz, and the dominant wave heading is longitudinal. Water depth is 50 m, with no forward speed included in diffraction calculations. These settings define a shallow-water, stationary first-order response model; they do not reproduce inland-route bathymetry or the encounter conditions of a vessel advancing at 5.4 knots.

Table 4. Natural modes reported for the modelled floating condition.

Mode	Frequency Hz	Period s	Damping %	Dominant response
1	0.37222	2.68661	5.53411	Pitch and heave
2	0.41381	2.41658	8.13416	Pitch and heave
3	0.45718	2.18734	2.78126	Roll
4	0.49480	2.02102	7.66265	Pitch and heave

The lightly damped roll mode at approximately 0.457 Hz identifies a response region requiring further attention in beam and oblique waves. The largest reported pitch response-amplitude operator is 8.62633 degrees per metre at 0.36673 Hz. The maximum roll response for the analysed longitudinal heading is only 0.17154 degrees per metre at 0.47994 Hz. These values cannot be transferred directly to other headings, particularly beam seas where transverse excitation is stronger. Reported added-mass coefficients vary sharply near the upper part of the frequency range, including negative values in some components. Such frequency-dependent coefficients are not physical negative vessel masses. Nevertheless, the extreme variation requires a mesh and frequency-resolution investigation before the associated response peaks are used for design. A mesh specification alone does not establish numerical convergence. For subsequent CFD calculations, ITTC (2024b) provides a verification and validation methodology that distinguishes numerical uncertainty from agreement with experimental observations.

The irregular-wave calculation uses a long-crested JONSWAP spectrum with peak enhancement factor 3.3, alpha 0.0081 and peak frequency 0.595 Hz. Its 1.68 s peak period is shorter than the dominant natural-mode periods. The 60 s simulation uses a 0.1 s step and reports small bounded motions, including surge extrema of approximately −1.70 and +1.67 mm. The exact spectrum scaling and realised significant wave height should be recovered before interpreting these values as operational conditions. The spectrum formulation originates from the wind-wave growth and swell-decay observations of Hasselmann et al. (1973); its use here does not establish that the selected parameters describe Okrika conditions. The spectrum peak also lies close to the upper analysed frequency of 0.60185 Hz. The represented high-frequency tail and its effect on spectral moments should therefore be checked. Small simulated motions may reflect the selected excitation and frequency representation; they are not proof that the craft would experience similarly small motions on the intended route.

The calculation omits forward-speed effects, nonlinear slamming, a complete second-order force treatment and viscous drag contributions. A short stationary simulation cannot establish passenger comfort, extreme loads, deck wetness or structural adequacy. The defensible result is identification of sensitive frequency bands and a numerically balanced initial condition, with route-specific seakeeping still outstanding. ITTC (2024a) recommends defining operational conditions, environmental inputs, mass properties and measurement procedures when planning seakeeping experiments.

Resistance and electrical propulsion demand

The recalculated resistance curve rises moderately at low speed and steeply once the assumed wave-making term becomes significant. At 5.4 knots, the Froude number is approximately 0.181 and total resistance is about 1.95 kN. Effective power is approximately 5.42 kW, delivered power

is 9.86 kW and electrical input is 11.17 kW. These values reproduce the reported operating-point result within rounding.

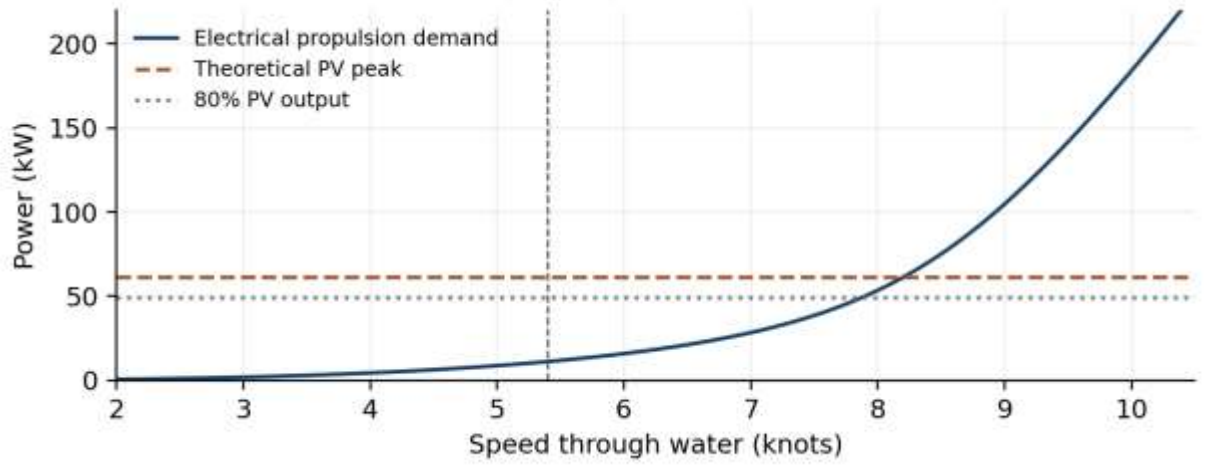


Figure 2. Reproduced electrical propulsion demand and photovoltaic power scenarios. The crossings exclude auxiliary loads and do not establish attainable speed with the fixed propeller setting.

Table 5. Recalculated calm-water performance at selected speeds.

Speed kn	Resistance kN	Effective kW	Delivered kW	Electrical kW
2.0	0.27	0.28	0.51	0.58
4.0	1.04	2.14	3.88	4.40
5.4	1.95	5.42	9.86	11.17
6.0	2.50	7.71	14.03	15.89
8.0	6.31	25.97	47.21	53.48
10.0	17.36	89.31	162.38	183.96
12.0	31.39	193.80	352.37	399.19

At 8 knots, electrical demand is approximately 53.48 kW; at 10 and 12 knots it rises to approximately 183.96 and 399.19 kW. The baseline 61.2 kW photovoltaic line intersects the electrical-demand curve at about 8.20 knots, while 48.96 kW intersects at about 7.87 knots. These are power-balance screening points under the assumed curve, not demonstrated maximum vessel speeds. The selected 5.4-knot point requires approximately 2.07 kWh per nautical mile for propulsion alone, compared with 6.69 kWh per nautical mile at 8 knots. Speed reduction therefore improves both instantaneous power balance and energy per distance in this model. The amount of improvement remains sensitive to the uncalibrated residual-resistance expression. Gorter (2015) likewise relates solar-racing-boat propeller selection to available photovoltaic energy. This supports matching propulsion demand to the available energy budget, without transferring racing-boat performance directly to the present catamaran.

Propeller matching and efficiency reconciliation

For two nominal 1.0 m propellers at 189 rpm, the calculated advance coefficient at 5.4 knots is about 0.7496. The illustrative polynomials give KT ≈ 0.1095, KQ ≈ 0.0186 and open-water efficiency η_0 ≈ 0.703. Available thrust slightly exceeds the hull requirement, and the curves intersect at approximately 5.44 knots.

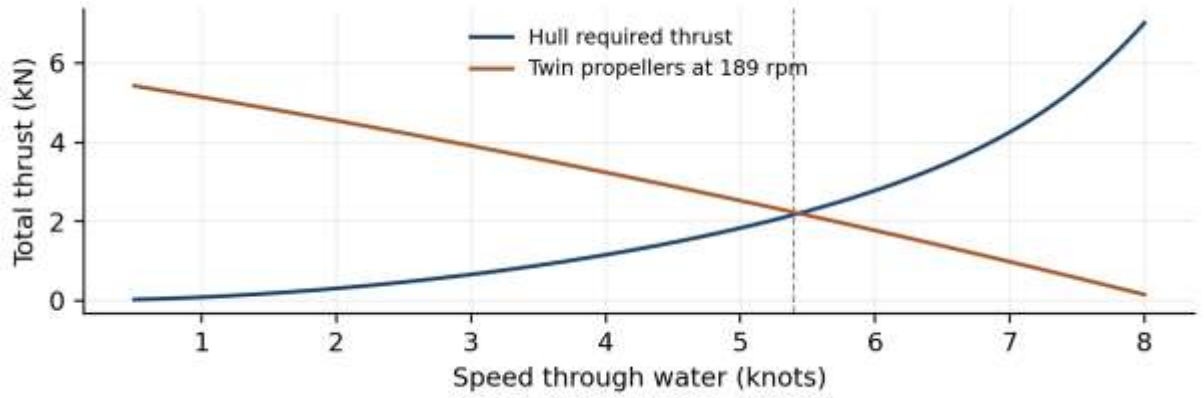


Figure 3. Reproduced thrust matching using the assumed open-water polynomials. The intersection is a numerical model result rather than an experimentally verified operating point.

Table 6. Preliminary matching results at the selected cruise speed.

Quantity	Approximate value
Required total thrust	2.168 kN
Available total thrust	2.227 kN
Available thrust margin	0.059 kN or 2.7%
Torque absorbed per propeller	188.93 N·m
Total propeller absorbed power	7.479 kW
Hull required delivered power with η_0 model	7.281 kW
Predicted matching speed	5.44 knots
Reduction from 1,000 rpm motor reference	5.29 to 1

The 7.281 kW delivered-power estimate differs from the 9.86 kW value in Table 5 because the two calculations use different propulsion efficiencies. With thrust deduction 0.10 and wake fraction 0.15, hull efficiency is $(1 - t)/(1 - w) = 1.059$. Multiplying by $\eta_0 \approx 0.703$ and an assumed relative rotative efficiency of unity gives approximately 0.744, whereas Table 5 uses a fixed coefficient of 0.55. The estimates are alternative model scenarios and should not be combined as though they came from one calibrated propulsion model. Molland, Turnock and Hudson (2017) distinguish effective power, delivered power and the individual efficiency factors, providing the basis for keeping these alternative estimates separate.

The small thrust margin at fixed rpm is insufficient evidence of reserve for fouling, waves, wind or asymmetric loading. A variable-speed operating map and verified propeller curves are required to establish torque limits and off-design capability. The 8-knot photovoltaic screening point also requires a different shaft operating condition; it cannot be achieved merely by supplying more power while retaining 189 rpm. The principal finding is conditional feasibility at moderate speed. The baseline solar-energy estimate exceeds modelled propulsion demand for an eight-hour cruise schedule on an average input day, but the result depends strongly on usable area, photovoltaic efficiency and the service pattern. The calculation does not show that all intended journeys can be completed without external charging. Energy autonomy requires time-resolved storage simulation, including return-leg requirements and adverse weather sequences.

An illustrative reduction to 22% photovoltaic efficiency and 80% coverage of the 204 m² envelope gives 35.90 kW peak capacity. With the same mean solar input and 0.80 yield factor, available generation becomes approximately 121.22 kWh/day. Under the August mean it falls to approximately 72.33 kWh/day. The illustrative eight-hour, 2 kW auxiliary-load schedule then has an August deficit of about 33.03 kWh/day before battery losses. This sensitivity demonstrates why cell efficiency and gross deck dimensions cannot substitute for an installation layout and manufacturer module ratings. De Soto, Klein and Beckman (2006) model photovoltaic performance under changing irradiance and temperature. Jordan and Kurtz (2013) additionally show why long-term output estimates should account for degradation rather than assume unchanged generation throughout service.

The electrical architecture also requires revision before equipment selection. A 61.2 kW source at 48 V corresponds to approximately 1,275 A before losses. A single 140 A device at that voltage represents only 6.72 kW; it cannot serve as the sole full-power path for the baseline array. Similarly, the 400 kVA inverter mentioned in the preliminary sizing material is not justified by the reconstructed propulsion load. Appropriate bus voltage, protection, conductor sizing, isolation, conversion equipment and battery management must follow a consistent load schedule.

Implications for the intended waterway

A 50 m hydrodynamic depth is representative evidence for an inland route. Local water depth, tidal currents, channel restrictions, traffic-generated waves and available under-keel clearance must be incorporated into the next design stage. A fixed speed over ground can require greater speed through water against a current, changing propulsion demand substantially. Travel time and range should therefore be calculated from a defined route rather than inferred from the cruise-speed figure alone. Payload and weight also remain unresolved. The preliminary description gives both ten and thirty passengers, and its passenger-mass total is inconsistent with its assumed mass per person. Consequently, the reported 57.96 t displacement must be supported by a component weight schedule covering hull, structure, propulsion, batteries, canopy, passengers and stores. Each loading case should be checked for draft, trim, centre of gravity and reserve buoyancy.

Validation priorities and research significance

The immediate priorities are to verify solar-data provenance; establish route and payload requirements; develop the module layout and electrical single-line design; and reconcile the resistance and propeller-efficiency assumptions. Resistance prediction should then be calibrated using suitable experiments or validated numerical analysis. Hydrostatic and seakeeping assessment should include mesh convergence, operational loading, shallow water, forward speed,

additional headings and realistic wave spectra. Prototype trials should measure speed, shaft torque, electrical input and battery state of charge.

Fuel displacement, emissions reduction and financial payback cannot be quantified from the available results. These outcomes require a reference combustion vessel, comparable duty cycle, fuel data, charging-source information and lifecycle cost assumptions. The present contribution is the identification of a testable design envelope and the assumptions that control it, allowing subsequent experiments and detailed engineering to address the most consequential uncertainties. Tercan et al. (2021) evaluate solar-boat alternatives using location-specific irradiation, energy losses and financial assumptions. Their approach supports undertaking a separate local feasibility analysis before assigning a payback period to this design.

4.0 Conclusions

A preliminary numerical assessment was developed for a 24 m × 8.5 m solar electric catamaran proposed for Okrika inland waterway. The reproduced resistance model predicts approximately 1.95 kN resistance and 11.17 kW electrical propulsion demand at 5.4 knots. The assumed twin 1.0 m propellers at 189 rpm match the modelled hull near 5.44 knots, but the fixed-speed thrust margin is only about 2.7% and the open-water curves remain unvalidated.

The theoretical 61.2 kW photovoltaic estimate gives approximately 258.29 kWh/day using the unweighted mean of the supplied solar matrix. Its lowest individual input yields only 79.56 kWh/day before losses. A more restrictive area-and-efficiency scenario reduces peak capacity to 35.90 kW, demonstrating the importance of installation geometry and realistic module ratings. Battery capacity and service availability cannot be finalised without a defined voyage schedule and time-resolved energy balance.

Reported hydrostatic results are internally consistent and indicate strong initial restoring stiffness. They do not establish large-angle stability or route-specific seaworthiness. Sensitive motion frequencies around 0.37–0.50 Hz, the deep-water assumption and the short simulation duration require further investigation. The evidence therefore supports continued development of a moderate-speed solar-assisted transport concept, subject to validation of the hull, propulsion, electrical installation and local operating conditions.

References

Bertram, V. (2012). Practical Ship Hydrodynamics (2nd ed.). Butterworth-Heinemann.

De Soto, W., Klein, S. A., & Beckman, W. A. (2006). Improvement and validation of a model for photovoltaic array performance. Solar Energy, 80(1), 78–88. https://doi.org/10.1016/j.solener.2005.06.010

Dobos, A. P. (2014). PVWatts Version 5 Manual. NREL/TP-6A20-62641. National Renewable Energy Laboratory. https://www.nrel.gov/docs/fy14osti/62641.pdf

Faltinsen, O. M. (2005). Hydrodynamics of High-Speed Marine Vehicles. Cambridge University Press.

Geertsma, R. D., Negenborn, R. R., Visser, K., & Hopman, J. J. (2017). Design and control of hybrid power and propulsion systems for smart ships: A review of developments. Applied Energy, 194, 30–54. https://doi.org/10.1016/j.apenergy.2017.02.060

Gorter, T. (2015). Design considerations of a solar racing boat: Propeller design parameters as a result of PV system power. Energy Procedia, 75, 1901–1906. https://www.sciencedirect.com/science/article/pii/S1876610215009479

Han, J., Charpentier, J.-F., & Tang, T. (2014). An energy management system of a fuel cell/battery hybrid boat. Energies, 7(5), 2799–2820. https://doi.org/10.3390/en7052799

Hasselmann, K., et al. (1973). Measurements of wind-wave growth and swell decay during the Joint North Sea Wave Project (JONSWAP). Deutsche Hydrographische Zeitschrift, Ergänzungsheft A(8), 12, 1–95.

International Towing Tank Conference. (2021a). 1978 ITTC Performance Prediction Method. Procedure 7.5-02-03-01.4, Revision 05. https://ittc.info/media/11796/75-02-03-014.pdf

International Towing Tank Conference. (2021b). Open Water Test. Procedure 7.5-02-03-02.1, Revision 04. https://www.ittc.info/media/9621/75-02-03-021.pdf

International Towing Tank Conference. (2024a). Seakeeping Experiments. Procedure 7.5-02-07-02.1, Revision 08. https://www.ittc.info/media/11888/75-02-07-021.pdf

International Towing Tank Conference. (2024b). Uncertainty Analysis in CFD Verification and Validation Methodology and Procedures. Procedure 7.5-03-01-01, Revision 05.

Jordan, D. C., & Kurtz, S. R. (2013). Photovoltaic degradation rates—An analytical review. Progress in Photovoltaics: Research and Applications, 21(1), 12–29. https://doi.org/10.1002/pip.1182

King, D. L., Boyson, W. E., & Kratochvil, J. A. (2004). Photovoltaic Array Performance Model. SAND2004-3535. Sandia National Laboratories. https://doi.org/10.2172/919131

Lewis, E. V. (Ed.). (1988). Principles of Naval Architecture (Second Revision). Society of Naval Architects and Marine Engineers.

Molland, A. F., Turnock, S. R., & Hudson, D. A. (2017). Ship Resistance and Propulsion: Practical Estimation of Ship Propulsive Power (2nd ed.). Cambridge University Press.

Moya, M., Martínez-Gómez, J., Urresta, E., & Cordovez-Dammer, M. (2022). Feature selection in energy consumption of solar catamaran INER 1 on Galapagos Island. Energies, 15(8), 2761. https://doi.org/10.3390/en15082761

Nasirudin, A., Chao, R.-M., & Utama, I. K. A. P. (2017). Solar powered boat design optimization. Procedia Engineering, 194, 260–267. https://doi.org/10.1016/j.proeng.2017.08.144

Nitonye, S. & Adumene, S., (2015). Predictive Analysis of Bare-Hull Resistance of a 25,000 DWT Tanker Vessel. *International Journal of Engineering and Technology, (IJET)* United Kingdom, 5 (4), 194-198. (http://www.ijet.journal.org).

Nitonye, S., Adumene, S., Sigalo, B. M., Orji, C. U. & Le-ol, A K (2020), *Dynamic Failure Analysis of Renewable Energy Systems in the Remote Offshore Environments*, Quality and Reliability Engineering International, https://onlinelibrary.wiley.com/doi/full/10.1002/qre.2805, **DOI:** https://doi.org/10.1002/qre.2805

Nwaorgu G.O and Ogbonnaya E. A. (2023). Evaluation of an Alternative Source of Power forShip Operations in Ports. Journal of Engineering, Emerging Technologies and AppliedSciences (JEETAS). 1(1), 2-12. *(PDF) design of a hybrid wave energy converter for escravos using phk-ros model*. Available from: https://www.researchgate.net/publication/399885264_DESIGN_OF_A_HYBRID_WAVE_ENERGY_CONVERTER_FOR_ESCRAVOS_USING_PHK-ROS_MODEL [accessed Nov 11 2026].

Schirripa Spagnolo, G., Papalillo, D., Martocchia, A., & Makary, G. (2012). Solar-electric boat. Journal of Transportation Technologies, 2(2), 144–149. https://doi.org/10.4236/jtts.2012.22015

Tercan, Ş. H., Eid, B., Heidenreich, M., Kogler, K., & Akyürek, Ö. (2021). Financial and technical analyses of solar boats as a means of sustainable transportation. Sustainable Production and Consumption, 25, 404–412. https://doi.org/10.1016/j.spc.2020.11.014